Extreme Mechanics Letters 1 (2014) 120–126

Contents lists available at ScienceDirect

Extreme Mechanics Letters

journal homepage: www.elsevier.com/locate/eml

Fabric-based stretchable electronics with mechanically optimized designs and prestrained composite substrates

Renxiao Xu [a,b,c,1], Kyung-In Jang [d,e,1], Yinji Ma [a,b,c,f], Han Na Jung [d,e], Yiyuan Yang [d,e], Moongee Cho [d,e], Yihui Zhang [a,b,c,f,*], Yonggang Huang [a,b,c], John A. Rogers [d,e,*]

[a] Departments of Civil and Environmental Engineering and Mechanical Engineering, Northwestern University, Evanston, IL 60208, USA
[b] Center for Engineering and Health, Northwestern University, Evanston, IL 60208, USA
[c] Skin Disease Research Center, Northwestern University, Evanston, IL 60208, USA
[d] Department of Materials Science and Engineering, University of Illinois at Urbana–Champaign, Urbana, IL 61801, USA
[e] Frederick Seitz Materials Research Laboratory, University of Illinois at Urbana–Champaign, Urbana, IL 61801, USA
[f] Center for Mechanics and Materials, Tsinghua University, Beijing 100084, China

ARTICLE INFO

Article history:
Received 2 December 2014
Received in revised form 23 December 2014
Accepted 23 December 2014
Available online 24 December 2014

Keywords:
Stretchable electronics
Serpentine interconnect
Finite element analyses
Prestrain
Fabric

ABSTRACT

A mechanically rugged form of stretchable electronics can be achieved through integration of functional materials and devices with composite substrates consisting of an ultralow modulus silicone adhesive layer on a strain-limiting fabric framework. The resulting system is sufficiently soft to enable extreme levels of deformation and non-invasive use on the skin, yet sufficiently robust for repetitive application/detachment. This letter introduces theoretical and experimental studies of mechanical designs, with optimization for a representative island-bridge device configuration to yield high levels of elastic stretchability. The physics of prestrain conversion and its role in enhancing the stretchability are systematically explored.

1. Introduction

Recent advances in mechanics and material science provide a foundation for stretchable/flexible electronics, in which high-performance devices can be combined with soft materials to allow for extreme levels of bending, twisting and stretching deformations without compromising the function of the system [1–9]. This technology creates new opportunities in bio-inspired engineering design and bio-integrated devices, with reported examples that range from functional artificial skins [10–14], to electronic eye-ball cameras [15–17], to in-vivo surgical instruments [18–20], and to "epidermal" (skin-based or-mounted) health monitors [21–24]. Mechanical stretchability in many of these systems [13–16,19,22,23] is achieved by adopting an "island-bridge design", where the functional components reside on the islands and the electrical interconnects form bridges to mechanically and electrically connect the islands. Because the islands are much stiffer than the bridges, stretchability is provided by the bridges almost completely. Quantitative mechanics modeling and design of deformable interconnects [16,19,23–34], therefore, plays a crucial role in the designs. The interconnects are often either fully bonded or not bonded at all to an underlying soft elastomeric substrate. Recently, Jang et al. [22] proposed a rugged form of stretchable electronics, where a composite substrate composed of an ultrasoft silicone coating as conformal, planarizing adhesive on a fabric layer that serves as a strain-limiting support. The resulting device combines ultralow modulus mechanics with high stretchability and high strength in a single

* Corresponding authors.
E-mail addresses: yihui.zhang2011@gmail.com (Y. Zhang), jrogers@illinois.edu (J.A. Rogers).

[1] These authors contributed equally to this work.

http://dx.doi.org/10.1016/j.eml.2014.12.010
2352-4316/

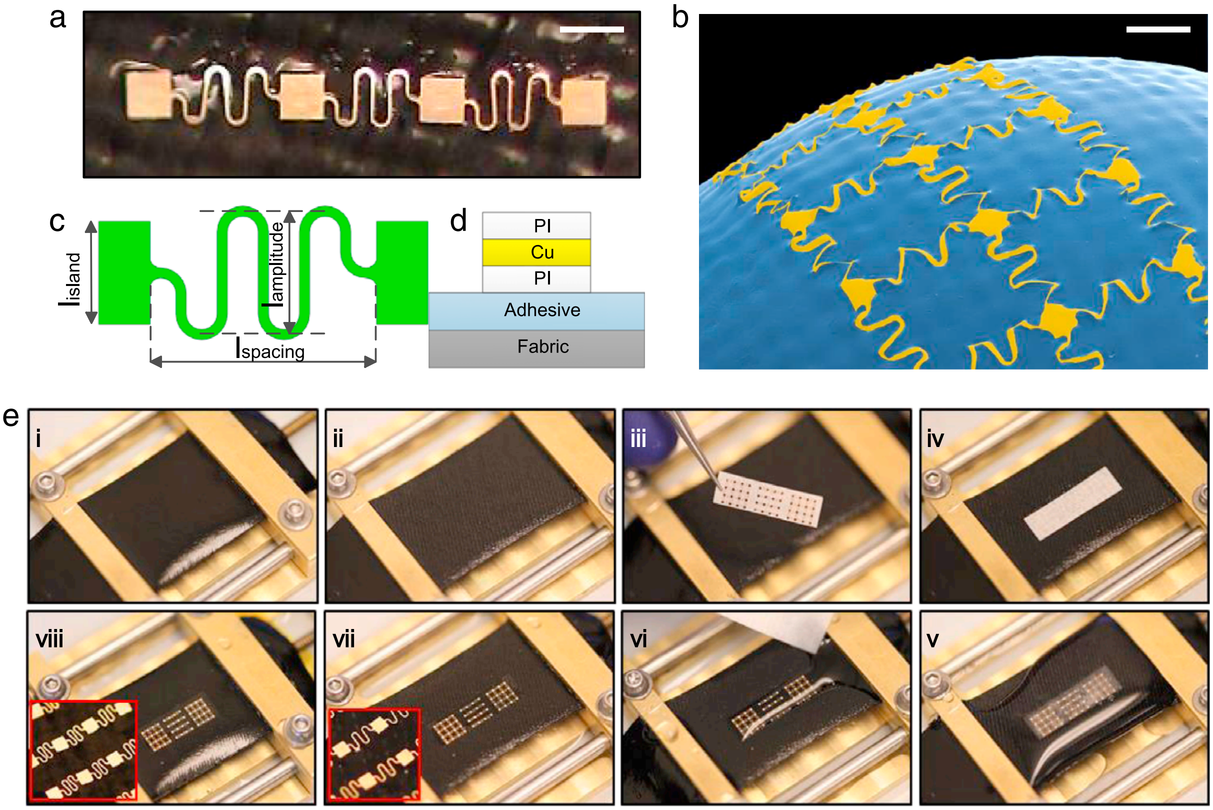

Fig. 1. Optical and SEM images of stretchable electronic structures bonded on substrate that consists of an ultralow modulus silicone coating on a stretchable fabric, arranged in (a) 1D chain and (b) 2D net configurations. Such patterns consist of repeated unit cells shown in (c). (d) Cross-sectional view of the system, highlighting both the circuit and the substrate. (e) Fabrication procedures for fabric-based stretchable electronics with 30% prestrain. The scale bars are 500 μm.

system, which not only facilitates non-invasive, conformal skin-integration, but also avoids strain-induced fractures that can otherwise occur during repetitive application and removal from the skin. This is because the ultrasoft silicone layer can accommodate the strain induced by application and removal processes without damage to circuits, while the stiffer fabric layer protects the system from excessive strain. The mechanics of this device system, however, can be quite different from those studied previously (e.g., serpentine interconnects bonded to a moderate soft (i.e., 60 kPa–1 MPa), single-layer substrate) [13,30,31,34,35], due to the use of an ultrasoft silicone layer (*Silbione* RT 4147 A/B, Bluestar Silicones, USA; modulus ∼3 kPa) that fully bonds to the circuits. In this letter, we present a mechanics study of such fabric-based stretchable electronic systems (with circuits, ultrasoft silicone adhesives, and fabric layers), aiming to provide guidelines for optimizing the circuit layout and key geometric parameters. The physics of using pre-strain in the substrate to achieve enhanced stretchability is further explored through combined finite element analysis (FEA) and experimental measurement. Generally, complex deformations (such as tension, bending and twisting) are involved in the devices taken on and off skin. In comparison to tensile deformation, the bending or twisting deformation of the device usually does not lead to considerable material strain, due to the ultrathin nature of the interconnect and the strain isolation of the ultralow modulus layer. Therefore, this paper focuses on the analyses of the island-bridge design under pure tensile deformation.

2. Results and discussions

Fig. 1(a) and (b) show layouts of a representative fabric-based stretchable circuit, suitable for conformal mounting on the skin for sensing parameters such as heart and muscle movement, brain activity, temperature, skin hydration, and so on. These layouts involve repetitions of a unit cell shown in Fig. 1(c) in one or two in-plane directions. The cell consists of two active components (islands) with side length l_{island}, separated by a distance $l_{spacing}$ and connected by a serpentine-shaped interconnect with amplitude $l_{amplitude}$ and width w. The metal layer (e.g., copper, ∼119 GPa) is sandwiched by two polyimide layers (PI, ∼2.5 GPa), and then mounted on a composite substrate made of rugged fabric (*Lycra*, The Yard, USA; modulus ∼391 kPa) that has a zigzag configuration of 90% of aliphatic polyamides and 10% of polyurethane–polyurea copolymer fibers, coated with a thin adhesive layer (e.g., *Silbione* RT Gel 4147 A/B, Bluestar Silicones, USA; modulus ∼3 kPa), as shown in Fig. 1(d). Due to the high degree of adhesion at the PI/substrate interface, the entire circuit is fully bonded to this composite substrate. Fig. 1(e) shows the sequence of fabrication procedures. The first step involves stretching a piece of fabric with a spin cast

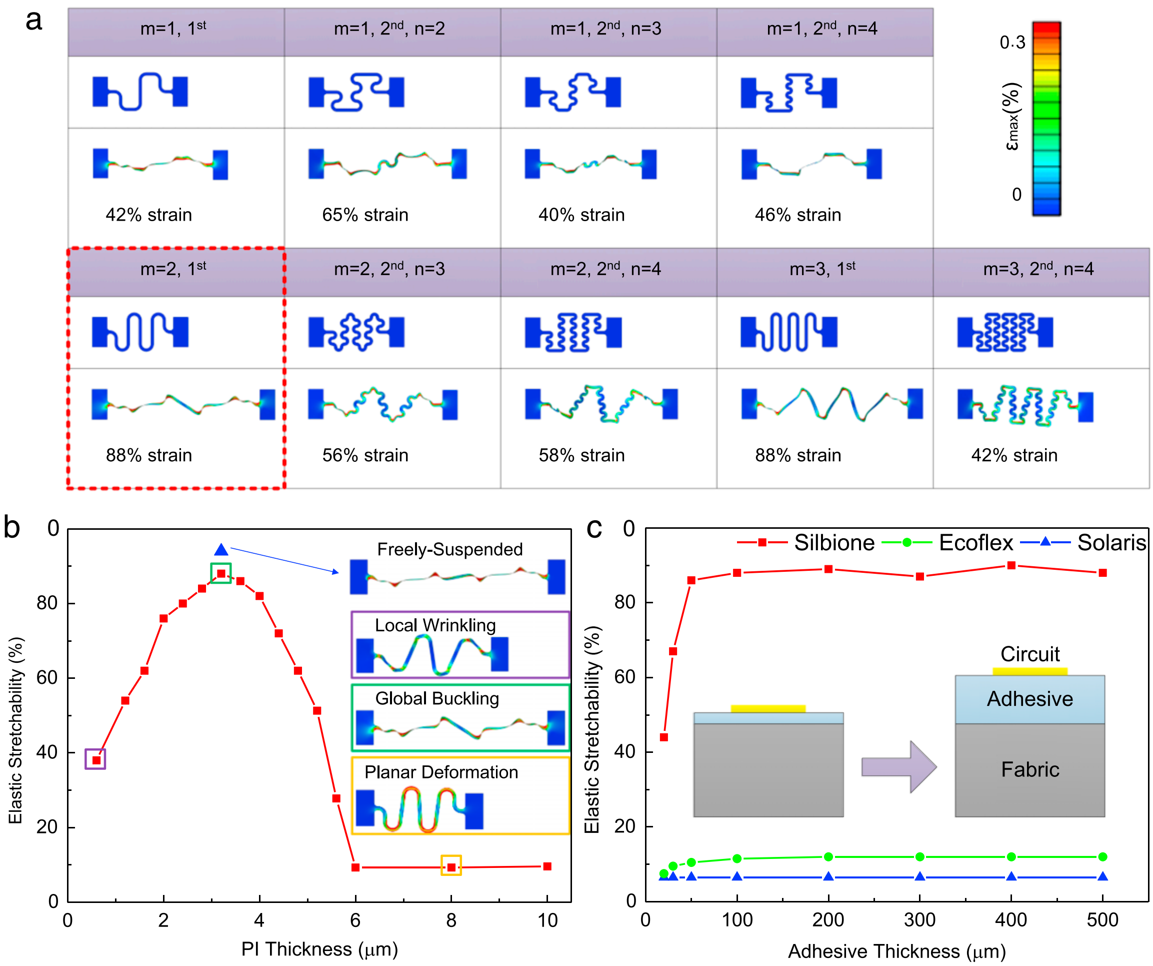

Fig. 2. FEA-guided optimization toward maximum elastic stretchability, taking into consideration (a) the planar geometry and the cross-section of (b) the circuit and (c) the composite. In Fig. 2(a), the circuit pattern in the red dashed box yields the highest elastic stretchability. The insets of Fig. 2(b) denote the deformed configurations at the corresponding limit of elastic stretchability. The three curves in Fig. 2(c) correspond to different adhesive materials. The color in Fig. 2(a) and (b) denotes the maximum principal strain in the metal.

ultrasoft silicone coating using a mechanical stage. Next, a piece of water soluble (cellulose) tape serves as a vehicle for transferring a pre-fabricated collection of electronic unit cells from a separate substrate to the stretched, silicone-coated fabric. Upon release of the applied strain, the integrated system deforms into 'prestrained structures' that provide enhanced stretchability.

To identify an optimized interconnect pattern that maximizes the elastic stretchability $\varepsilon_{elastic0}$ (defined by the yield strain of copper, ∼0.3%), we employed three-dimensional (3D) FEA to analyze the deformation and strain distribution of the system under stretching. The elastic stretchability is determined based on the criterion when the maximum principal strain exceeds the yield strain at half the width of any certain section in the wire-shaped interconnect. The validity of this criterion has been proved by previous experimental studies [34,36] using both cyclic mechanical testing and four-probe resistance measurements. In the design optimization of interconnect pattern, the thickness of the composite substrate is fixed, e.g., as $t_{Adhesive} = 100$ μm, $t_{Fabric} = 1$ mm, [22] and prestrain is not used. The optimized serpentine layout is determined by comparing the stretchabilities of various possible patterns (including the self-similar serpentine) that fit into a prescribed area ($l_{spacing}$ by $l_{amplitude}$) between two adjacent islands. We take a representative net layout adopted by Jang et al. [22] as an example to illustrate the optimization. The key geometric parameters in this layout include, $l_{island} =$ 400 μm, $l_{spacing} =$ 880 μm, and $l_{amplitude} =$ 600 μm, selected partly to avoid interference among differently oriented interconnects during deformation. Under the geometric constraint that the rounding radius should be larger than half of the interconnect width, nine representative patterns can be constructed (in Fig. 2(a)), for a typical interconnect width, $w = 40$ μm. The generation of these patterns involves changes in the number (m) of unit cells for the serpentine backbone (with $l_{amplitude} = 600$ μm) fitted into the space between islands, and if applicable, the number (n) of unit cells in the serpentine microstructures. The FEA results (in Fig. 2(a)) demonstrate that longer interconnects with more serpentine microstructures (e.g., $m = 3$ and $n = 4$) do not necessarily yield higher $\varepsilon_{elastic0}$ given the same spacing. This behavior is different from that of typical cases of freely suspended serpentine interconnects [27]. The differences arise from effects of mechanical constraint imposed by the adhesive layer on the interconnects, despite its ultralow modulus. For a more tightly distributed interconnect (i.e., with a further increased unit number, m and n), the strain concentration due to small rounding radius plays a major role, leading to reduced elastic stretchability. On the other hand, short interconnects (e.g., $m = 1$, 1st order) are also deficient due to their inferior geometrical capacity for stretching. The optimized pattern ($m = 2$, 1st order) represents a compromise between the length and complexity of the interconnect, thereby yielding the highest $\varepsilon_{elastic0} = 88\%$. For this pattern, the failure sections reside at the four arc regions of the interconnect, rather than the connection point between interconnect and metallic island, as shown in supplementary Fig. S1. This further demonstrates the rationality of this optimized pattern. When m further increases to 3 for the 1st order interconnect, $\varepsilon_{elastic0}$ no longer increases, even though the electrical resistance (proportional to the length of interconnect) continues to increase. Based on this consideration, the interconnect pattern in the dashed box of Fig. 2(a) is taken as the optimal solution, and is adopted in the following analyses.

While the elastic stretchability of the interconnect is primarily defined by its planar layout, the cross-sectional design (in Fig. 1(d)), such as the thickness of PI clad and adhesive layer, is also important. Fig. 2(b) shows that increasing the thickness of PI clad (from 0.6 to 10 μm) increases the elastic stretchability gradually to a maximum at ∼3.2 μm, and then decreases it until a trough is approached (starting from ∼6.0 μm). Such thickness dependence can be mainly attributed to transitions in the mode of deformation in the serpentine interconnect. For a relatively thin PI clad (e.g., ∼0.6 μm), the interconnect undergoes local wrinkling, as shown in the inset of Fig. 2(b), because of the relatively small out-of-plane bending stiffness. In this scenario, the radius of curvature due to out-of-plane bending is small at the sites of the wrinkles, which leads to a large local strain in metal, and therefore, a relatively low elastic stretchability. For a moderately thick PI clad (e.g., 3.2 μm), no wrinkling occurs, and the serpentine interconnect undergoes purely global buckling. Since this type of deformation mode resembles that of a freely suspended interconnect, as shown in Fig. 2(b), the resulting elastic stretchability (∼88%) is also close to the theoretical limit (∼94% for the freely suspended interconnect). For a relatively thick PI clad (e.g., 8.0 μm), the serpentine interconnect is governed by planar, in-plane bending deformations, due to an interconnect thickness that becomes comparable to the width. In this regime, the elastic stretchability is tremendously reduced to ∼10%, and becomes independent of the PI thickness, as expected for pure planar deformations. It is noteworthy that the stretchability during this regime can be enhanced by narrowing the width of interconnect, according to theoretical results obtained by Zhang et al. [26] and Widlund et al. [28].

Fig. 2(c) illustrates the effect of the composite substrate on the elastic stretchability of the interconnects, for thicknesses of the adhesive layer $t_{Adhesive}$ between 20 and 100 μm. Considering the relatively large thickness (e.g., >0.5 mm) of the fabric layer and the strain-isolating effects of the adhesive layer, the thickness of the fabric has negligible effect on the stretchability, and is thus fixed as 1.0 mm in the calculation. When the adhesive layer is very thin (e.g., ∼30 μm), the fabric sets a physical barrier on buckling motions of the interconnects, resulting in a severely reduced elastic stretchability, as illustrated in Fig. 2(c). When the thickness of the adhesive layer exceeds a critical saturation value $t_{Adhesive\text{-}crit}$ (50–100 μm), the interconnects are almost completely isolated from the influence of fabric layer, leading to an elastic stretchability that is insensitive to changes in $t_{Adhesive}$. It is noteworthy that this thickness-dependent saturation phenomenon only exists in conformal substrates with an adhesive layer that is sufficiently soft to enable considerable out-of-plane deformation in interconnect. If the ultralow modulus (*Silbione*, ∼3 kPa) layer is replaced by the widely-used elastomers with higher moduli (e.g., *Ecoflex*, ∼60 kPa or *Solaris*, ∼170 kPa), such effects will be reduced, as shown in Fig. 2(b), because of the planar-dominated or pure planar deformation of island-bridge circuit in the circuit/*Ecoflex*/fabric or circuit/*Solaris*/fabric system. The elastic stretchability is substantially reduced (by a factor larger than 7) by replacement of *Silbione* with *Ecoflex* or *Solaris*.

Further enhancements in the elastic stretchability are possible by pre-straining ($\varepsilon_{pre\text{-}applied}$) the composite substrate prior to mounting the electronics. To examine the effects, deformations in a chain of island-bridge structures with different numbers of unit cells (ranging from 1 to 10) were analyzed during the release of the pre-strain. Fig. 3(a) presents the converted pre-strain ($\varepsilon_{pre\text{-}absorbed}$) in each periodic unit of a chain with k cells (i.e., consisting of k interconnects and $(k + 1)$ islands), for $\varepsilon_{pre\text{-}applied} = 30\%$. The results clearly show effects of the boundaries. Specifically, $\varepsilon_{pre\text{-}absorbed}$ is significantly smaller than $\varepsilon_{pre\text{-}applied}$ for the unit cells near the edges (i.e., the first and last) of each chain, while in contrast, this parameter is very close to $\varepsilon_{pre\text{-}applied}$ at unit cells in the middle of the chain. SEM images and FEA results in Fig. 3(b) illustrate the underlying physics of these boundary effects. The islands at the ends of the chains have interconnects only on one side, whereas all other islands are connected at both sides. As such, the island at each end will be subject to an out-of-plane shear deformation (as evidenced in Fig. 3(b)) relative to the soft substrate upon release of the pre-strain, resulting in a reduced pre-strain conversion at the boundary. This finding is different from that in previous studies of the use of pre-strain, where no clear boundary effects were observed in systems consisting only of serpentine patterns (i.e., without islands) [34]. It is also noteworthy that the enhancement of elastic stretchability due to the use of prestrain cannot be achieved by adopting a relaxed, planar serpentine layout that mimics the in-plane geometry of shrunken interconnect after prestrain release, as demonstrated in supplementary Fig. S2.

The incomplete absorption of pre-strain (due to the boundary effect) can be modulated by adjusting the thickness of the PI clad, as supported by the computational results in Fig. 3(c), in which the pre-strain conversion of two-island chains with the same planar geometry

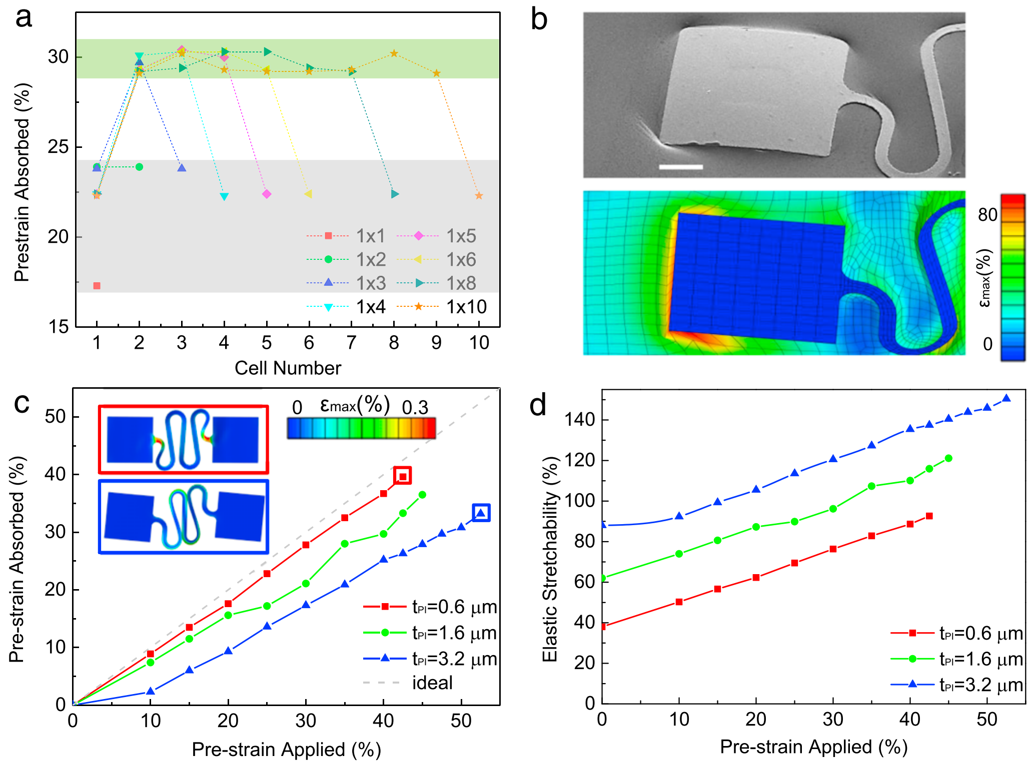

Fig. 3. (a) Absorbed prestrain in each unit cell of chains with different numbers of cells for the case of 30% prestrain and PI thickness of 3.2 µm. The results indicate a clear boundary effect, where interconnects near the edge of the chain are less effective in prestrain absorption. (b) SEM image (scale bar ∼100 µm) and corresponding FEA featuring the shear deformation of an island in relative to the soft substrate. (c) Absorbed prestrain and (d) elastic stretchability of the interconnect as a function of applied prestrain for a two-island chain with three representative PI clad thicknesses. The color in Fig. 3(b) and (c) denotes the maximum principal strain in the substrate and the metal, respectively.

were studied. Generally, the effectiveness of the pre-strain conversion can be characterized by a dimensionless coefficient η as

$$\eta = \varepsilon_{pre\text{-}absorbed}/\varepsilon_{pre\text{-}applied}, \quad (1)$$

which also denotes the secant slope of each data point on the curves. Fig. 3(c) demonstrates that circuits with thicker PI clads (e.g., $t_{PI} = 1.6$ µm or 3.2 µm) and consequently, higher tensile stiffness are less effective in pre-strain conversion than thinner samples (e.g., $t_{PI} = 0.6$ µm). As the applied pre-strain increases, the effectiveness of the pre-strain conversion (η) for circuits with thin PI clads (e.g., 0.6 µm) approaches a constant at ∼1. Increasing the $\varepsilon_{pre\text{-}applied}$ can yield an increased $\varepsilon_{pre\text{-}absorbed}$, which enhances the elastic stretchability of the circuit. Generally, there exists an upper limit for the amount of pre-strain convertible for a circuit, i.e., $\varepsilon_{pre\text{-}absorbed\text{-}max}$, which is defined by two different criteria for circuits having thinner and thicker PI clads, as illustrated in the insets of Fig. 3(c). In the case with thicker PI clads (e.g., $t_{PI} = 1.6$ µm or 3.2 µm), the serpentine interconnect undergoes out-of-plane deformation while being compressed until it starts to overlap. Since this overlapping can cause an undesirable, irreversible adhesion among the interconnects and the adjacent silicone layer, $\varepsilon_{pre\text{-}absorbed\text{-}max}$ is defined as the maximum $\varepsilon_{pre\text{-}absorbed}$ before observable overlapping. When the PI clad is thin, however, the local wrinkling behavior of interconnects can accommodate the energy from pre-strain and prevent the interconnects from overlapping. In such cases, $\varepsilon_{pre\text{-}absorbed\text{-}max}$ is defined as the maximum $\varepsilon_{pre\text{-}absorbed}$ without plastic yielding of metal. Fig. 3(d) illustrates the enhancement of elastic stretchability as a function of pre-strain for three different PI thicknesses. After using the pre-strain, the interconnects with thicker PI clads (i.e., 3.2 µm) still offer convincingly higher $\varepsilon_{elastic}$, and correspond to the optimal design, because of the significant advantage that originates from the deformation mode of global buckling.

The boundary effect described above is validated quantitatively by experimental results in Fig. 4, through comparison of deformations in each unit cell of a four-island chain, during the compression process related to release of pre-strain (30%). The FEA results agree well with SEM images (Fig. 4(b)). Both indicate that the absorbed pre-strain (∼23.8%) at the edge unit cells is clearly lower than that (∼29.7%) at the middle unit cell. After the release of pre-strain, the composite substrate is stretched in experiment until the elastic limit (predicted by FEA) is reached in the bonded circuits. The complex buckling deformations in such island-bridge chain structure are shown in Fig. 4(c), in which good agreement can be observed between FEA and SEM images. According to FEA calculations, the elastic stretchability is 131.8% for the entire four-island chain, while locally ∼126.3% and ∼143.2% for the unit cells at the edge and middle, respectively. In comparison, neglecting the boundary effect gives a uniform elastic stretchability (144.4%), thereby resulting in ∼14.3% (relatively)

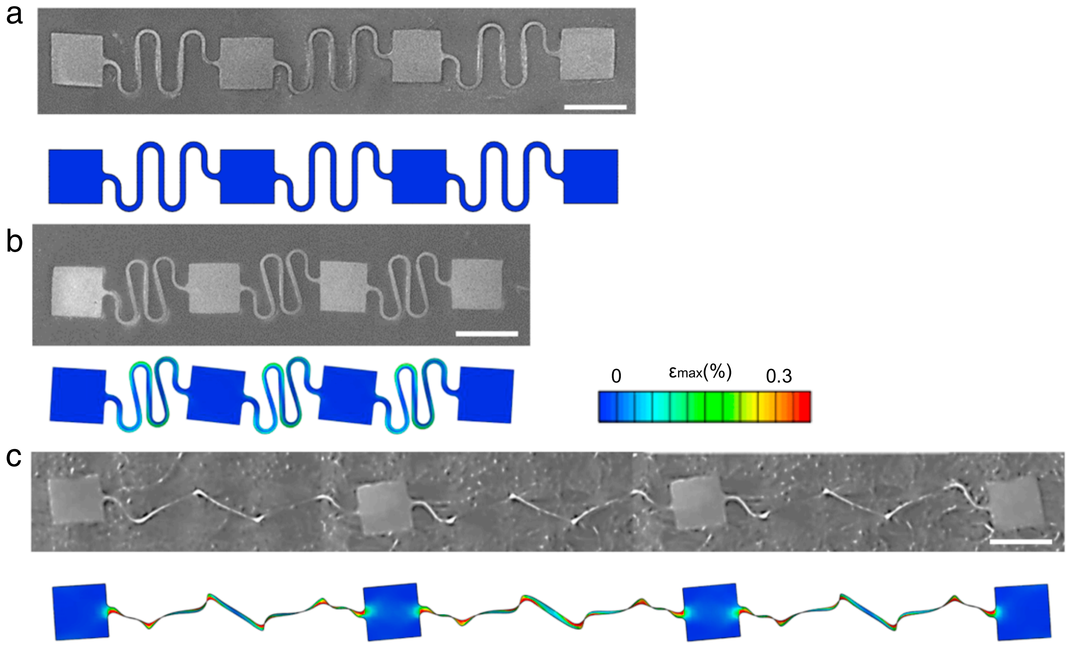

Fig. 4. Experimental and FEA results of a four-island chain (a) mounted on a substrate with 30% prestrain, (b) after prestrain release and (c) stretched to the elastic limit. The color denotes the maximum principal strain in metal. The scale bars are 500 μm.

over-estimation of elastic stretchability for the edge unit cells, which could be an important consideration in practical applications.

3. Conclusions

In summary, the work presented here describes fundamental mechanical design considerations for fabric-based stretchable electronics, where the goal is to optimize the elastic stretchability. Strategies that involve prestrain applied to the substrate are examined by combined FEA and experiment, which reveals a boundary effect in the conversion of prestrain from the substrate to circuits with island-bridge layouts. The reported systematic optimization procedures and the mechanics of boundary effects are important for future work in stretchable electronics, especially for practical systems that include large periodic arrays of device components.

Acknowledgments

Work at University of Illinois was supported by the US Department of Energy (DOE), Office of Science, Basic Energy Sciences (BES) under Award # DOE DE-FG02-07ER46471. Y.H. acknowledges the support from National Science Foundation (DMR-1121262 and CMMI-1400169). K.-I. Jang acknowledges the support from a Basic Science Research Program through the National Research Foundation of Korea (NRF) funded by the Ministry of Education (D00008).

Appendix A. Supplementary data

Supplementary material related to this article can be found online at http://dx.doi.org/10.1016/j.eml.2014.12.010.

References

[1] S.P. Lacour, J. Jones, S. Wagner, T. Li, Z.G. Suo, Proc. IEEE 93 (2005) 1459.
[2] D.Y. Khang, H.Q. Jiang, Y. Huang, J.A. Rogers, Science 311 (2006) 208.
[3] S.P. Lacour, S. Wagner, R.J. Narayan, T. Li, Z. Suo, J. Appl. Phys. 100 (2006) 014913.
[4] H. Jiang, D.-Y. Khang, J. Song, Y. Sun, Y. Huang, J.A. Rogers, Proc. Natl. Acad. Sci. USA 104 (2007) 15607.
[5] H. Jiang, D.-Y. Khang, H. Fei, H. Kim, Y. Huang, J. Xiao, J.A. Rogers, J. Mech. Phys. Solids 56 (2008) 2585.
[6] T. Sekitani, H. Nakajima, H. Maeda, T. Fukushima, T. Aida, K. Hata, T. Someya, Nature Mater. 8 (2009) 494.
[7] J.A. Rogers, T. Someya, Y. Huang, Science 327 (2010) 1603.
[8] S. Yang, N. Lu, Sensors 13 (2013) 8577.
[9] Y. Huang, Y. Duan, Y. Ding, N. Bu, Y. Pan, N. Lu, Z. Yin, Sci. Rep. 4 (2014) 5949.
[10] T. Someya, T. Sekitani, S. Iba, Y. Kato, H. Kawaguchi, T. Sakurai, Proc. Natl. Acad. Sci. USA 101 (2004) 9966.
[11] S. Wagner, S.P. Lacour, J. Jones, P.H.I. Hsu, J.C. Sturm, T. Li, Z.G. Suo, Physica E-Low-Dimens. Syst. Nanostruct. 25 (2004) 326.
[12] D.J. Lipomi, M. Vosgueritchian, B.C.K. Tee, S.L. Hellstrom, J.A. Lee, C.H. Fox, Z.N. Bao, Nature Nanotechnol. 6 (2011) 788.
[13] N. Lu, C. Lu, S. Yang, J. Rogers, Adv. Funct. Mater. 22 (2012) 4044.
[14] S. Park, H. Kim, M. Vosgueritchian, S. Cheon, H. Kim, J.H. Koo, T.R. Kim, S. Lee, G. Schwartz, H. Chang, Z. Bao, Adv. Mater. 26 (2014) 7324.
[15] H.C. Ko, M.P. Stoykovich, J. Song, V. Malyarchuk, W.M. Choi, C.-J. Yu, J.B. Geddes III, J. Xiao, S. Wang, Y. Huang, J.A. Rogers, Nature 454 (2008) 748.
[16] Y.M. Song, Y. Xie, V. Malyarchuk, J. Xiao, I. Jung, K.-J. Choi, Z. Liu, H. Park, C. Lu, R.-H. Kim, R. Li, K.B. Crozier, Y. Huang, J.A. Rogers, Nature 497 (2013) 95.
[17] C.C. Huang, X.D. Wu, H.W. Liu, B. Aldalali, J.A. Rogers, H.R. Jiang, Small 10 (2014) 3050.
[18] Z. Yu, O. Graudejus, C. Tsay, S.P. Lacour, S. Wagner, B. Morrison III, J. Neurotrauma 26 (2009) 1135.
[19] D.-H. Kim, N. Lu, R. Ghaffari, Y.-S. Kim, S.P. Lee, L. Xu, J. Wu, R.-H. Kim, J. Song, Z. Liu, J. Viventi, B. de Graff, B. Elolampi, M. Mansour, M.J. Slepian, S. Hwang, J.D. Moss, S.-M. Won, Y. Huang, B. Litt, J.A. Rogers, Nature Mater. 10 (2011) 316.
[20] D.-H. Kim, S. Wang, H. Keum, R. Ghaffari, Y.-S. Kim, H. Tao, B. Panilaitis, M. Li, Z. Kang, F. Omenetto, Y. Huang, J.A. Rogers, Small 8 (2012) 3263.

[21] G. Schwartz, B.C.K. Tee, J. Mei, A.L. Appleton, D.H. Kim, H. Wang, Z. Bao, Nature Commun. 4 (2013) 1859.
[22] K.-I. Jang, S.Y. Han, S. Xu, K.E. Mathewson, Y. Zhang, J.-W. Jeong, G.-T. Kim, R.C. Webb, J.W. Lee, T.J. Dawidczyk, R.H. Kim, Y.M. Song, W.-H. Yeo, S. Kim, H. Cheng, S.I. Rhee, J. Chung, B. Kim, H.U. Chung, D. Lee, Y. Yang, M. Cho, J.G. Gaspar, R. Carbonari, M. Fabiani, G. Gratton, Y. Huang, J.A. Rogers, Nature Commun. 5 (2014) 4779.
[23] D. Son, J. Lee, S. Qiao, R. Ghaffari, J. Kim, J.E. Lee, C. Song, S.J. Kim, D.J. Lee, S.W. Jun, S. Yang, M. Park, J. Shin, K. Do, M. Lee, K. Kang, C.S. Hwang, N. Lu, T. Hyeon, D.-H. Kim, Nature Nanotechnol. 9 (2014) 397.
[24] S. Xu, Y.H. Zhang, L. Jia, K.E. Mathewson, K.I. Jang, J. Kim, H.R. Fu, X. Huang, P. Chava, R.H. Wang, S. Bhole, L.Z. Wang, Y.J. Na, Y. Guan, M. Flavin, Z.S. Han, Y.G. Huang, J.A. Rogers, Science 344 (2014) 70.
[25] S. Xu, Y. Zhang, J. Cho, J. Lee, X. Huang, L. Jia, J.A. Fan, Y. Su, J. Su, H. Zhang, H. Cheng, B. Lu, C. Yu, C. Chuang, T.-I. Kim, T. Song, K. Shigeta, S. Kang, C. Dagdeviren, I. Petrov, P.V. Braun, Y. Huang, U. Paik, J.A. Rogers, Nature Commun. 4 (2013) 1543.
[26] Y. Zhang, H. Fu, Y. Su, S. Xu, H. Cheng, J.A. Fan, K.-C. Hwang, J.A. Rogers, Y. Huang, Acta Mater. 61 (2013) 7816.
[27] Y. Zhang, S. Xu, H. Fu, J. Lee, J. Su, K.-C. Hwang, J.A. Rogers, Y. Huang, Soft Matter 9 (2013) 8062.
[28] T. Widlund, S. Yang, Y.-Y. Hsu, N. Lu, Internat. J. Solids Structures 51 (2014) 4026.
[29] T. Li, Z.G. Suo, S.P. Lacour, S. Wagner, J. Mater. Res. 20 (2005) 3274.
[30] M. Gonzalez, F. Axisa, M.V. Bulcke, D. Brosteaux, B. Vandevelde, J. Vanfleteren, Microelectron. Reliab. 48 (2008) 825.
[31] Y.-Y. Hsu, M. Gonzalez, F. Bossuyt, F. Axisa, J. Vanfleteren, I. De Wolf, J. Mater. Res. 24 (2009) 3573.
[32] J. Song, Y. Huang, J. Xiao, S. Wang, K.C. Hwang, H.C. Ko, D.H. Kim, M.P. Stoykovich, J.A. Rogers, J. Appl. Phys. 105 (2009) 123516.
[33] Y. Zhang, H. Fu, S. Xu, J.A. Fan, K.-C. Hwang, J. Jiang, J.A. Rogers, Y. Huang, J. Mech. Phys. Solids 72 (2014) 115.
[34] Y. Zhang, S. Wang, X. Li, J.A. Fan, S. Xu, Y.M. Song, K.-J. Choi, W.-H. Yeo, W. Lee, S.N. Nazaar, B. Lu, L. Yin, K.-C. Hwang, J.A. Rogers, Y. Huang, Adv. Funct. Mater. 24 (2014) 2028.
[35] D.H. Kim, N.S. Lu, R. Ma, Y.S. Kim, R.H. Kim, S.D. Wang, J. Wu, S.M. Won, H. Tao, A. Islam, K.J. Yu, T.I. Kim, R. Chowdhury, M. Ying, L.Z. Xu, M. Li, H.J. Chung, H. Keum, M. McCormick, P. Liu, Y.W. Zhang, F.G. Omenetto, Y.G. Huang, T. Coleman, J.A. Rogers, Science 333 (2011) 838.
[36] J.A. Fan, W.-H. Yeo, Y.W. Su, Y. Hattori, W. Lee, S.-Y. Jung, Y.H. Zhang, Z.J. Liu, H.Y. Cheng, L. Falgout, M. Bajema, T. Coleman, D. Gregoire, R.J. Larsen, Y. Huang, J.A. Rogers, Nature Commun. 5 (2013) 3266.